LANGMUIR

pubs.acs.org/Langmuir Article

# 2D Colloids: Size- and Shape-Controlled 2D Materials at Fluid−Fluid Interfaces

David M. Goggin and Joseph R. Samaniuk*

Cite This: *Langmuir* 2021, 37, 14157−14166 Read Online

ACCESS | Metrics & More | Article Recommendations | Supporting Information

**ABSTRACT:** Advances in synthesis of model 3D colloidal particles with exotic shapes and physical properties have enabled discovery of new 3D colloidal phases not observed in atomic systems, and simulations and quasi-2D studies suggest 2D colloidal systems have an even richer phase behavior. However, a model 2D (one-atom-thick) colloidal system has yet to be experimentally realized because of limitations in solution-phase exfoliation of 2D materials and other 2D particle fabrication technologies. Herein, we use a photolithography-based methodology to fabricate size- and shape-controlled monolayer graphene particles, and then transfer the particles to an air−water interface to study their dynamics and self-assembly in real-time using interference reflection microscopy. Results suggest the graphene particles behave as "hard" 2D colloidal particles, with entropy influencing the self-assembled structures. Additional evidence suggests the stability of the self-assembled structures manifests from the edge-to-edge van der Waals force between 2D particles. We also show graphene discs with diameters up to 50 $\mu$m exhibit significant Brownian motion under optical microscopy due to their low mass. This work establishes a facile methodology for creating model experimental systems of colloidal 2D materials, which will have a significant impact on our understanding of fundamental 2D physics. Finally, our results advance our understanding of how physical particle properties affect the interparticle interactions between monolayer 2D materials at fluid−fluid interfaces. This information can be used to guide the development of scalable synthesis techniques (e.g., solution-phase processing) to produce bulk suspensions of 2D materials with desired physical particle properties that can be used as building blocks for creating thin films with desired structures and properties via interfacial film assembly.

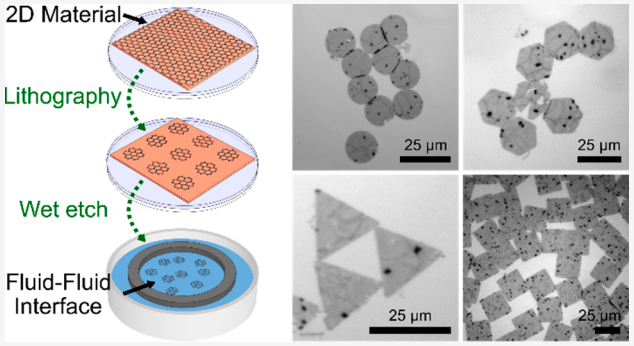


## INTRODUCTION

Systems of monodisperse three-dimensional (3D) colloidal particles have been extensively used as model systems for understanding bulk phenomena such as crystallization,[1] melting,[2] other 3D phase transitions,[3−5] and even surface phenomena such as capillary waves.[6] This is due in large part to the size of colloidal particles, which are large enough to be visualized with optical microscopy but small enough that Brownian dynamics still drive the system to evolve on reasonable observational time scales.[7,8] While there are many system parameters that can be tuned to control the interactions between colloidal particles,[9] a combination of particle shape[10−13] and system confinement[14−17] can lead to various self-assembled structures. This phenomenon is even more pronounced when there is confinement to a 2D plane. For example, Mason et al. demonstrated how Brownian cubes transitioned through several crystalline phases at high particle densities when confined to a pseudo-2D environment,[14] Thapar et al. used Monte Carlo simulations of various polyhedral particles in a 2D plane to understand how purely entropic interactions affected the phase behavior as a function of particle shape at high particle densities,[18] Murray et al. discovered that ∼5 nm thick lanthanide fluoride nanoplatelets assembled into films with different lattice structures at an air-ethylene glycol interface depending on the ratio of the faceted side lengths and the coverage of ligands due to directional interactions,[19] and Glotzer et al. used Monte Carlo simulations to understand the melting transitions of hard 2D polygons.[20] Although these works constitute progress in attempting to understand the relevant physics governing 2D colloidal systems through experiments and simulations, the experimental systems studied were 3D colloidal particles confined to pseudo-2D environments and the Monte Carlo simulations lacked dynamical information. Thus, there are still unanswered questions regarding how nanoscale interactions influence the dynamics and thermodynamics of truly 2D colloidal systems,

Received: September 14, 2021
Revised: November 8, 2021
Published: November 19, 2021

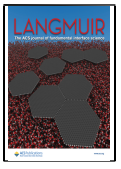







https://doi.org/10.1021/acs.langmuir.1c02418
*Langmuir* 2021, 37, 14157−14166

with the lack of model 2D colloidal systems for experimentation in this area being a significant limiting factor. In this work we propose a model experimental system that is two-dimensional at the atomic scale, that is, the particles are only one atom thick, and those particles are immersed in a 2D fluid medium, a fluid−fluid interface.

2D materials such as graphene, molybdenum disulfide ($MoS_2$), and hexagonal boron nitride (h-BN) represent an interesting class of anisotropic particles because they generally have colloidal-scale lateral dimensions, but thicknesses at the (sub)nanometer scale. Thus, relevant interactions at both of these scales can drive the interactions between 2D material particles depending on their relative orientation (i.e., face-to-face, edge-to-edge, face-to-edge) in the surrounding immersion media. When confined to a fluid−fluid interface, 2D materials are irreversibly trapped with their basal planes parallel to the interface,[21−24] which forces neighboring particles to interact in an edge-to-edge manner. This gives rise to a potential competition between colloidal particle-like and nanoparticle-like interactions present in 2D colloidal systems, and as we have previously noted,[25] it is still not understood if forces common in 3D colloidal particles at interfaces such as capillary, electrostatic, and van der Waals forces drive 2D colloid dynamics, if forces prevalent in nanoparticles at interfaces such as Casimir-like thermal fluctuations (i.e., capillary waves), line tension, entropy-driven interactions, and other $\sim 10^0$ $k_BT$-scale forces drive dynamics, or if there is a nonlinear combination of all these forces that needs to be better understood.[26] A system of model, monodisperse 2D particles of controlled shape and size would thus be highly valuable for a systematic investigation of this competition. However, a significant limitation inherent in the common solution-phase processing methods currently used to create suspensions of 2D materials is the polydispersity of the resulting particles with respect to size, shape, and thickness.

In this work, we report the fabrication and transfer of size- and shape-controlled monolayer graphene particles to an air−water interface for use as a model 2D colloidal system. The photolithography-based fabrication technique enables control over particle thickness, shape, and size (down to ∼5 $\mu$m lateral dimensions), with future improvements in lateral resolution possible through electron beam lithography.[27] The ability to control the thickness, shape, and size of colloidal 2D materials has yet to be demonstrated using other 2D particle fabrication techniques, such as solution-phase exfoliation. After transfer of the particles from their growth substrate to an air−water interface, we use an optical microscopy technique known as interference reflection microscopy (IRM)[25,28] to directly visualize the dynamics and self-assembly of our size- and shape-controlled monolayer graphene particles. We find laterally aggregated particles remain intact even after deposition from an air−water interface onto a solid substrate, suggesting the attractive van der Waals (vdW) force between particles is strong enough to overcome disruptive forces associated with film drying. An expression for the edge-to-edge vdW force between two monolayer graphene discs is derived using a 2D Derjaguin approximation[29] to support this claim. Particle tracking results demonstrate that significant Brownian motion can be observed for monolayer graphene particles up to 50 $\mu$m in lateral size at an air−water interface, with measured diffusivities comparable to diffusivities reported for spherical nanoparticles at a fluid−fluid interface that are more than 2 orders of magnitude smaller in lateral dimension (diameter = 0.3 $\mu$m).[30] Finally, we use the radial distribution function and the global bond orientational order parameter, two common structural analysis tools, as quantifiable metrics to understand how particle size and shape influence the assembled film structure, respectively. We find monolayer graphene particles appear to exhibit hard 2D particle-like behavior, with entropy maximization based on particle size and shape influencing self-assembly. Future work aimed at identifying other possible interactions present in this system (e.g., Casimir-like,[31] shape-induced capillary,[32] etc.) would be useful to understand why these 2D particles occasionally deviate from true hard-particle behavior. Our work combines the use of top down (photolithography) and bottom-up (particle self-assembly) approaches to produce functional thin films with morphologies that can be manipulated via 2D particle size, shape, thickness, or chemistry. This ability to manipulate the physical properties of colloidal 2D materials creates an opportunity to construct lateral van der Waals heterostructure[33] thin film morphologies[34] that are difficult to achieve in chemical vapor deposition (CVD) grown 2D material films, and had yet to be realized until now because of limitations in solution-phase exfoliation[35−37] and 2D particle fabrication technology. This work overcomes these limitations. We expect our work will have a significant impact on the understanding of the colloidal and nanoscale forces driving self-assembly in 2D colloidal systems, and more broadly provides a methodology to create model thin film systems to investigate other applied and fundamental nanoscale physics, such as how the physical properties of interparticle junctions between 2D materials affect device performance[38] and reliability,[39] or how molecules orient themselves when interacting with the edges or basal plane of 2D materials for various applications.[40,41]

## EXPERIMENTAL SECTION

**Materials.** Monolayer graphene samples grown through chemical vapor deposition on Cu foils were purchased from Graphenea Inc. (San Sebastián, Spain). Polydimethylsiloxane (PDMS) base and curing agent (Dow SYLGARD 184 Silicone Encapsulant Kit, Ellsworth Adhesives, Germantown, WI) were mixed in a 7:1 base to curing agent ratio and degassed in a vacuum oven. Glass slides (Cat. No. 3011, Thermo Scientific, Waltham, MA) were cut into 25 mm × 25 mm squares and cleaned with acetone (ACS reagent), ethanol (ACS reagent), and ultrapure water (18.2 MΩ·cm, PURELAB Ultra Analytical purification unit, ELGA LabWater, UK) prior to spreading a PDMS layer to cure. Positive tone photoresist (AZ 1512, EMD Performance Materials) and alkaline developer (AZ 300 MIF, EMD Performance Materials) were purchased from Integrated Micro Materials (Argyle, TX). Ammonium persulfate (APS, ACS reagent grade, ≥98%) was purchased from Sigma-Aldrich and added to ultrapure water for a solution concentration of 0.25 M APS. Acetone and ethanol (ACS reagent grade) were purchased from Pharmco-Aaper and used for cleaning purposes. 1-Methyl-2-pyrrolidone (NMP, biotech. grade, ≥99.7%) was purchased from Sigma-Aldrich and was used for removing photoresist.

**Sample Preparation and Particle Fabrication.** Substrates of PDMS on glass were prepared by gently spreading degassed PDMS onto each square glass slide and then curing the PDMS at 150 °C. Graphene was removed from the backside of all graphene samples prior to processing using RIE with parameters of 30 W power, 200 mTorr operating pressure, 40 sccm (standard cubic centimeters per minute) Ar gas, 10 sccm $O_2$ gas, and 90 s total etching time. Pieces of the parent graphene on Cu (G@Cu) sample were cut into ∼8.5 mm × 8.5 mm squares, placed in the center of a PDMS on glass substrate, and gently flattened using a clean glass slide. Photoresist was then added in excess to the G@Cu sample without overflow from the edge


https://doi.org/10.1021/acs.langmuir.1c02418
Langmuir 2021, 37, 14157−14166

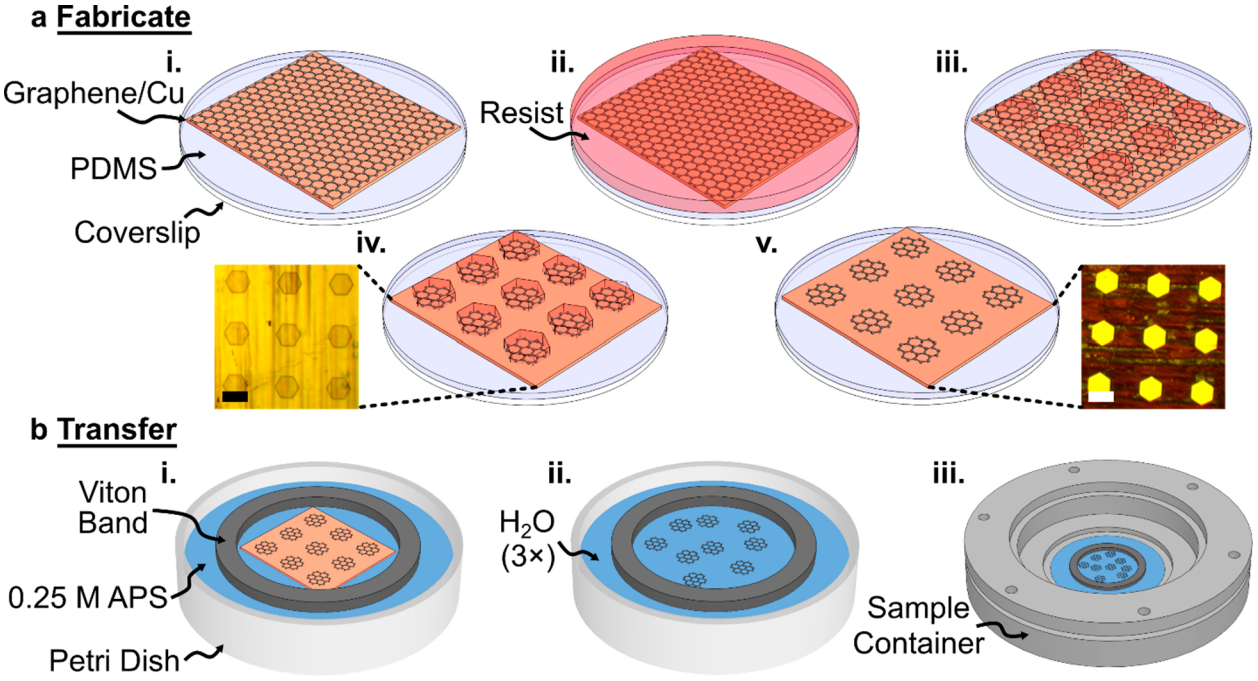


**Figure 1.** Schematic of particle fabrication process and transfer to an air−water interface. (a) i. Prepare sample for photolithography. ii. Spin-coat photoresist onto sample. iii. Exposure and development of photoresist. iv. Remove exposed graphene through reactive ion etching. v. Remove photoresist with NMP. Inset images are optical images of samples after processing at stage (iv) and after stage (v). Scale bars in inset images are 50 $\mu$m. (b) i. Place patterned sample within a Viton band on the surface of 0.25 M ammonium persulfate (APS) etching solution. ii. Clean the sample three times in fresh water baths after Cu is etched away. iii. Place sample in sample container for imaging with interference reflection microscopy.

of the PDMS on glass substrate and then spin-coated using a three-step process: (1) 500 rotations per minute (rpm), 25 rpm/s acceleration, 40 s total time, (2) 1000 rpm, 50 rpm/s acceleration, 40 s total time, (3) 4000 rpm, 200 rpm/s acceleration, 80 s total time. Excess photoresist was then removed with an acetone swab and samples were soft baked at 100 °C for 60 s. A chromium-on-glass photomask (<2 $\mu$m critical dimension, Front Range Photomask, Lake Havasu City, AZ) was used to pattern samples with the desired features. Hard contact between the photoresist-covered sample and photomask was made, and exposure to UV light was accomplished with a SUSS MJB3 mask aligner (Karl Suss, Germany). Exposure dosages varied depending on the desired particle shape and size, with day-to-day variances in equipment performance requiring a test run to confirm particle integrity. General exposure dosages of ∼100 mJ/cm$^2$ (5 $\mu$m particles), ∼125 mJ/cm$^2$ (10 $\mu$m particles), ∼200 mJ/cm$^2$ (25 $\mu$m particles), and ∼250 mJ/cm$^2$ (50 $\mu$m particles) were used as the starting point and iterated if particle integrity was subpar. Particles were slightly smaller than the features on the photomask because of slight overexposure. Immediately after UV exposure, samples were developed in AZ 300 MIF developer for 45−60 s under mild agitation, rinsed with ultrapure water, and dried with $N_2$ gas.

Lithographically patterned samples were then subjected to another round of RIE (30 W, 200 mTorr, 40 sccm Ar, 10 sccm $O_2$, 90 s etch time) to remove graphene not covered by photoresist. Finally, the patterned regions of photoresist were removed from the G@Cu samples by soaking the samples in hot NMP (∼80 °C) for 10 min, followed by a cleaning of the samples using acetone and ethanol baths (1 min each), and finally three different water baths (5 min each). Samples were then allowed to air-dry before removing the backside Cu foil and transferring the size- and shape-controlled graphene particles to an air−water interface following the procedure in our previous work.[25]

**Image Acquisition.** Images were acquired using the same interference reflection microscopy setup used in our previous work.[25] Images in Figure 2a−d,f, Figure 3a−d, Figure 4a, and Figure 6a were acquired using a 40× objective (Nikon CFI Apochromat NIR, water-immersion, NA = 0.80), the inset image in Figure 3e and the image in Figure 4c and Figure 6b (same image) were acquired using a 10× objective (Nikon Plan Fluor, NA = 0.30), and the image in Figure 6c was acquired at a total magnification of 15× using the 10× objective with the 1.5× intermediate magnification enhancement setting on the microscope. Exposure time was adjusted accordingly to maximize image contrast and clarity.

**Raman Spectroscopy.** The sample of 10 $\mu$m discs shown in Figure 2f was deposited from an air−water interface onto a Si wafer with a 300 nm oxide layer (University Wafers, Boston, MA) by scooping the sample out of the interface and allowing it to dry overnight. The Raman map in Figure 2g shows the intensity of the G peak (I(G)) at ∼1580 cm$^{-1}$ and intensity of the D peak (I(D)) at ∼1350 cm$^{-1}$, represented by green and red hues, respectively. The map was acquired with a WITec Alpha 300R Confocal/Raman microscope (Germany). Image scan was set to a 50 $\mu$m × 50 $\mu$m square with 166 pts/line, 166 lines/image, 33.2 s/line (trace), and 33.2 s/line (retrace).

**Particle Tracking.** Images obtained for particle tracking measurements (Figure 3e,f) were acquired at 68.11 frames per second (1024 × 1024 pixels, 10 ms exposure) for 10 001 frames. Particle tracks were analyzed using the MATLAB algorithm originally developed by Crocker and Grier[42] and later modified by Samaniuk and Vermant[43] to calculate relative MSD as a function of lag time for particles at fluid−fluid interfaces. Relative MSD calculates the relative displacements between pairs of particles and effectively eliminates particle drift, which would result in greater than expected displacements, from the data.[43] The reported relative MSD values were acquired from the six particles (14 particle pairs) shown in Figure 3e,f and represent the ensemble time average.

**Self-Assembled Structure Analysis.** A custom MATLAB script (R2020a) was written to analyze the morphology in Figure 4a,c. Images were imported and centroids were identified using the "imfindcircles" built-in MATLAB function. Six of the identified centroids were then manually selected for each image that resided in the center of the image. The radial distribution function was calculated for each image by finding the number density of centroids within a given annular area a certain distance from the particle of


https://doi.org/10.1021/acs.langmuir.1c02418
Langmuir 2021, 37, 14157−14166

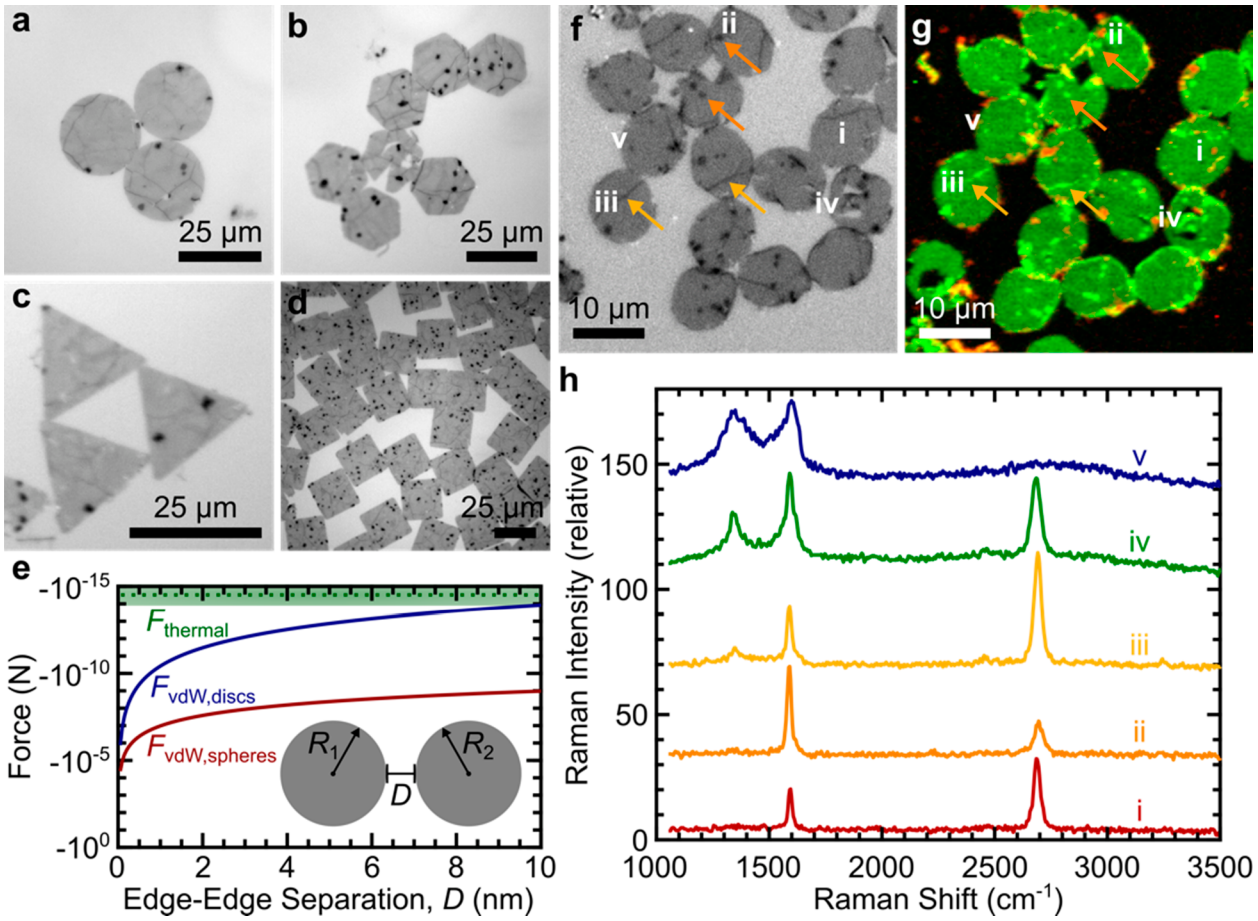


**Figure 2.** Shape-controlled particles at an air−water interface. IRM images acquired in real time of 25 $\mu$m (a) discs, (b) hexagons, (c) triangles, and (d) squares assembled at an air−water interface. (e) van der Waals force between two discs with radii $R_1$ and $R_2$ interacting edge-to-edge as a function of the edge-to-edge separation, $D$ (blue curve), the van der Waals force between two spheres[29] of the same $R_1$ and $R_2$ (red curve), and the average thermal force[48] experienced by the particles in our system due to bombardment of the solvent molecules (dashed green line and faded green region). (f) IRM image of 10 $\mu$m discs assembled at an air−water interface before deposition to a solid substrate. Dark spots within particles (orange arrows) correspond to regions of multilayer graphene that formed during the CVD growth process and thin dark lines (yellow arrows) are line defects. (g) Raman map of the same assembly of 10 $\mu$m discs in (f) after deposition from the air−water interface onto a Si wafer with 300 nm oxide layer. (h) Individual Raman spectra corresponding to the locations labeled in (f,g): i. Monolayer graphene, ii. Multilayer graphene, iii. Monolayer graphene with a defect, iv. Residual photoresist located at the edge of a particle, v. Spectrum of residual photoresist.

interest and comparing that to the bulk number density. Annular regions were incremented by a distance dr = $R/10$ $\mu$m to a final annular region having a radius of 10$R$. Here, $R$ is the radius of the 10 or 50 $\mu$m particle, respectively. This normalization enabled direct comparison between particles of different size. The 2D FFT images were calculated using the built-in MATLAB functions "fft2" and "fftshift".

An extension of the custom MATLAB script (R2020a) was written to analyze the morphologies in Figure 6a−c. Images were first imported into FIJI (Fiji Is Just ImageJ, NIH) and processed as follows: subtract background (200 pixel or 500 pixel rolling ball radius, Figure 6a,c, respectively), enhance contrast (0.3%), adjust brightness/contrast (auto). Centroids were identified using the "imfindcircles" built-in MATLAB function for Figure 6b and manually identified for Figure 6a,c. The global bond order parameters $\Psi_3$, $\Psi_4$, and $\Psi_6$ were calculated using the following relation:

$$\Psi_n = \frac{1}{N}\left|\sum_{j=1}^{N}\frac{1}{n_j}\sum_{k=1}^{n_j}\exp(in\theta_{jk})\right| \quad (1)$$

where $N$ is the total number of particles, $n_j$ is the number of nearest neighbors for particle $j$, $n$ = 3, 4, or 6, and $\theta_{jk}$ is the angle made between particle $j$ and its nearest neighbor $k$ with respect to an arbitrary axis. For $\Psi_3$ and $\Psi_4$, the three or four closest neighbors to each particle were used for $n_j$, respectively, and for $\Psi_6$, $n_j$ was calculated using a Voronoi tessellation.[13] The Voronoi diagram was generated using the built-in MATLAB function "voronoin".

## RESULTS AND DISCUSSION

**Particle Fabrication and Transfer to Fluid−Fluid Interfaces.** Size- and shape-controlled monolayer graphene particles were patterned using the process shown schematically in Figure 1a. A film of monolayer molybdenum disulfide ($MoS_2$) was also patterned using a similar procedure to demonstrate the applicability to other 2D materials (Supporting Information). A layer of polydimethylsiloxane (PDMS) was first drop-cast on ~625 mm$^2$ glass slides to hold samples of monolayer graphene grown on Cu foil in place (Figure 1a,i) during photoresist spin-coating (Figure 1a,ii). Use of PDMS instead of conventional adhesives to hold the Cu foil during processing prevented undesirable polymeric residues from an adhesive that could later contaminate the fluid−fluid interface. Photoresist-coated samples were then aligned under a chromium photomask, exposed to UV light, and developed in an alkaline developer solution (Figure 1a,iii). A positive photoresist resulted in removal of photoresist from the UV-


https://doi.org/10.1021/acs.langmuir.1c02418
Langmuir 2021, 37, 14157−14166

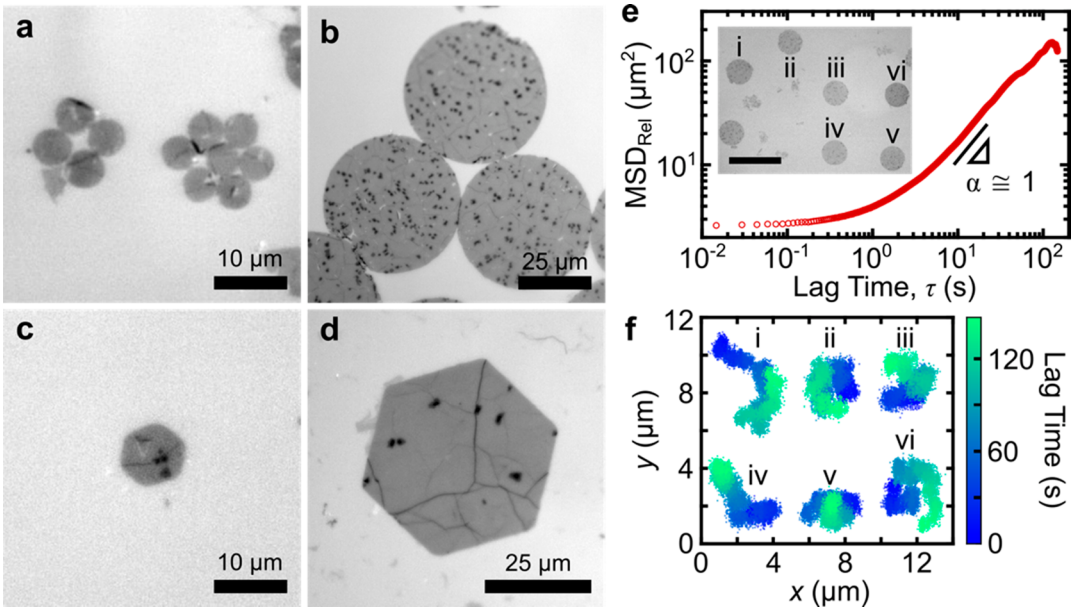


**Figure 3.** Size-controlled particles at an air−water interface. IRM images of (a) 5 $\mu$m diameter discs, (b) 50 $\mu$m diameter discs, (c) 10 $\mu$m hexagons, and (d) 50 $\mu$m hexagons at an air−water interface. Dark spots within particles correspond to regions of multilayer graphene and thin dark lines are line defects. (e) Ensemble and time averaged relative mean-squared displacement ($MSD_{Rel}$) as a function of lag time $\tau$ for a set of 50 $\mu$m discs (14 total pairs of particles tracked). Solid line shows a slope of 1 between lag times of 10 and 20 s indicative of diffusive behavior. There are 206 and 103 independent observations at lag times of 10 and 20 s, respectively. Inset image shows an IRM image of the six particles tracked; scale bar is 100 $\mu$m. (f) Individual tracks of particles i−vi in (e). Each point depicts the center point of each particle at the corresponding lag time, given by the color scale along the right side of (f).

exposed regions in alkaline developer after exposure. Exposed graphene was removed via reactive ion etching (RIE) in a mixture of Ar and $O_2$ plasma (Figure 1a,iv). We note the chemistry of the plasma could be used to induce functionalization of the particle edges or surface,[44] but was not investigated here. Particle chemistry was studied before and after all processing steps with Raman spectroscopy, and results are discussed in more detail in the "Particles at an Air−Water Interface" section. Remaining photoresist was then removed to reveal size- and shape-controlled monolayer graphene particles on the original Cu foil (Figure 1a,v). Particles were released from the Cu foil and transferred to a fluid−fluid interface following a protocol similar to our previous work[25] (Figure 1b). Briefly, a patterned, graphene-on-Cu foil sample was placed within a confining band on the surface of a 0.25 M ammonium persulfate (APS) etching solution (Figure 1b,i). After the Cu foil was etched, the band and particles were transferred to three different water baths to remove residual APS (Figure 1b,ii), and then to an air−water interface in a custom sample chamber[45] (Figure 1b,iii) for observation with an inverted optical microscope operating in IRM mode.[25]

**Particles at an Air−Water Interface.** Monolayer graphene discs, hexagons, triangles, and squares (25 $\mu$m lateral dimension) were observed as individual particles and also found to form a variety of structures once at an air−water interface (Figure 2a−d). We note that local area concentrations evolve from diffusion-limited aggregation, but the global area concentration can be controlled during the particle fabrication stage via the density of particles on the photomask or with a Langmuir trough.[45] Assembled structures remained intact with no particle detachment for the duration of observation, which implies the magnitude of the attractive force between particles is significant at length scales less than the resolution of optical microscopy (<300 nm). Particles were also not observed to stack on top of one another, consistent with our previous work.[46] In that work, which focused on a molecular dynamics study of 2D particle stacking, microscopy images of shape-controlled particles were included to support simulation results, but no details of particle fabrication or analysis of self-assembly were included. Given the simplistic chemistry of graphene and the apparent intimate contact between particles, the dominant force at this length scale is likely van der Waals. The van der Waals force between two circular graphene discs $F_{vdW,discs}$ was derived using a 2D Derjaguin approximation[29] and is given by (derivation in Supporting Information)

$$F_{vdW,discs} = \frac{-15A_H h^2 \sqrt{\left(\frac{R_1 R_2}{R_1 + R_2}\right)}}{256\sqrt{2}D^{7/2}} \quad (2)$$

where $A_H \sim 1 \times 10^{-19}$ J is the Hamaker constant,[47] $h$ the thickness of a graphene monolayer (0.34 nm), $R_i$ the radius of particle $i$, and $D$ the edge-to-edge separation between particles. We assumed $R_1 \approx R_2 \gg D$ and the particles could only interact in 2D (i.e., edge-to-edge). The blue curve in Figure 2e shows the results of eq 2 assuming $R_1 = R_2 = 12.5$ $\mu$m and the red curve shows the van der Waals force between two spheres $F_{vdW,spheres}$,[29] assuming the same values of $A_H$, $R_1$, and $R_2$. Three results are immediately noticeable: $F_{vdW,discs}$ decays more rapidly with separation than $F_{vdW,spheres}$, $F_{vdW,discs} \ll F_{vdW,spheres}$ at all separations, and $F_{vdW,discs}$ is extremely short-ranged before its magnitude is of the same order as thermal forces $F_{thermal}$; the magnitude of $F_{thermal}$ in this system can be estimated using the fluctuation−dissipation theorem.[48,49] These results are reasonable considering van der Waals forces are calculated by summing the energies of all atoms in one particle with all atoms in the other, and there are significantly fewer atoms


https://doi.org/10.1021/acs.langmuir.1c02418
Langmuir 2021, 37, 14157−14166

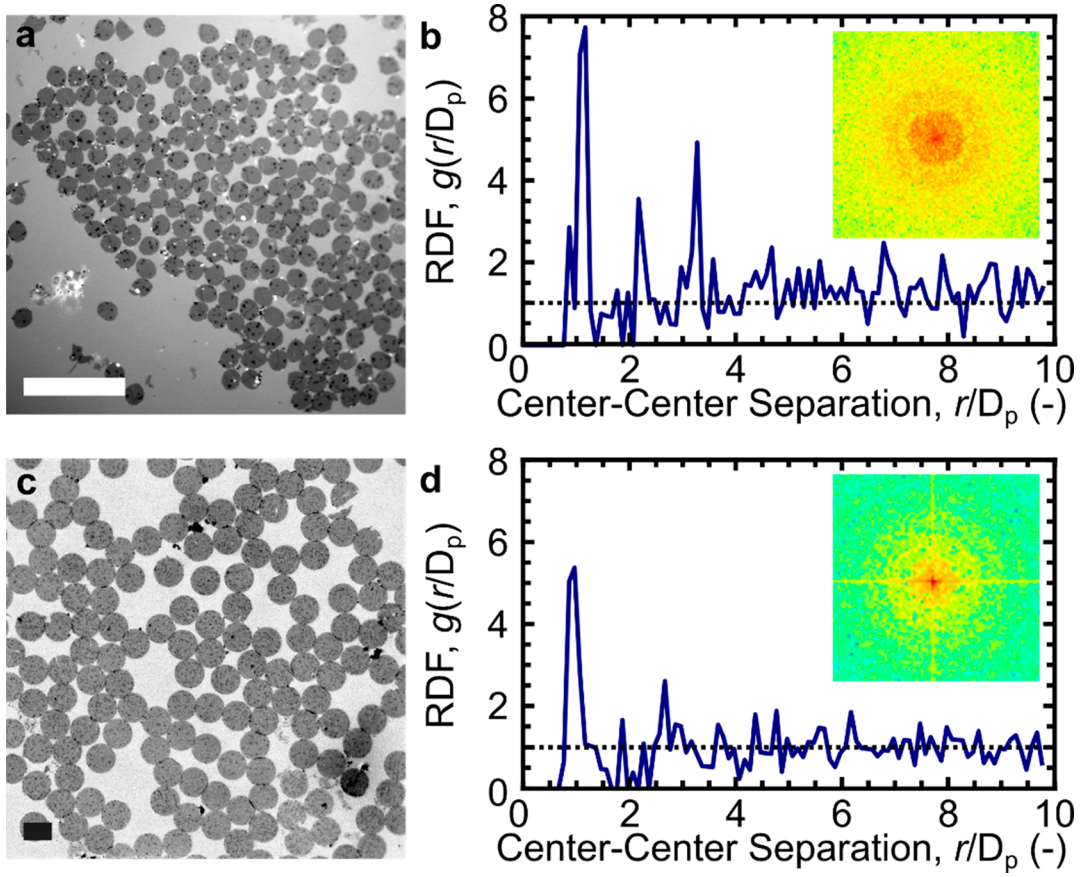


**Figure 4.** Analysis of self-assembled structures for different particle sizes. (a,c) IRM images of 10 $\mu$m (a) and 50 $\mu$m (c) monolayer graphene discs at an air−water interface. Scale bars are 50 $\mu$m. (b,d) Radial distribution function as a function of dimensionless center-to-center separation distance calculated for the images in (a,c), respectively. Inset images in (b,d) are the 2D FFT images of the IRM images in (a,c), respectively.

interacting at a given separation distance in disc-like particles than spherical particles. Additionally, a Bond number analysis of the system (Supporting Information), a dimensionless parameter describing the ratio of gravitational to capillary forces,[50] yields a value of $\sim 10^{-11}$ suggesting attractive long-range capillary interactions induced by monopolar deformations of the interface are negligible. Contact-line deformations due to physical particle properties such as edge roughness, chemical heterogeneities, or shape could also induce long-range capillary interactions.[50] However, the subnanometer thickness of monolayer graphene particles puts an order-of-magnitude upper limit on the maximum attractive interaction of $\sim 10^{-1} - 10^{1}\ k_B T$ at particle contact with optimal alignment, with the interaction magnitude decaying rapidly with separation distance due to the interaction potential scaling with separation distance to (approximately) the inverse fourth power.[51,52] Thus, the lack of significant long-range and only very short-range attractive forces makes our 2D particles potential candidates for an experimental "hard" disc system.[13]

Particles imaged at an air−water interface were also deposited onto a solid substrate for further characterization. It is significant that the interfacial structure observed at the air−water interface remained intact after deposition and drying despite the large forces that act on particles during evaporative processes. This observation indicates that the particles are likely in intimate contact as the magnitude of the attractive van der Waals forces in the self-assembled structures is sufficient (Figure 2e) to allow their transfer from an air−water interface to a solid substrate. Maintaining such structure during transfer is not always possible, and there is long-standing debate over the effect deposition has on the original interfacial structure present in various systems, for example, surfactant, particle, polymer, at fluid−fluid interfaces.[53] The undamaged deposited structures enabled us to obtain a Raman map of the particles and to compare those results with the corresponding IRM image to understand what the various features observed under IRM (Figure 2a−d,f), that is, dark spots and dark lines, are composed of. This analysis is shown in Figure 2f−h, and indicates that the particles observed using IRM were unoxidized graphene monolayers (Figure 2h,i),[25,44] with various multilayer regions that formed during the CVD growth process (dark spots, Figure 2h,ii),[25,28] line defects (thin dark lines, Figure 2h,iii),[54] and remnants of residual photoresist (Figure 2h,iv and Figure 2h,v). Understanding where regions of pristine, monolayer graphene versus functionalized, defect-rich, or multilayer graphene exist, especially near edges of particles, will enable future work investigating how various edge defects could be used as "sticky" or "patchy" regions to direct particle−particle interactions.[55,56]

The size of particles could also be varied (Figure 3a−d). Large polygons (Figure 3d) and disc-shaped particles with diameters from 5−50 $\mu$m (Figure 3a,b) displayed good shape integrity (i.e., the desired shapes on the photomask were successfully transferred to the photoresist and graphene monolayer with minimal size and shape distortion), but small polygons had rounded corners and edges (Figure 3c). The lateral sizes of particles produced in this work are governed by (1) the minimum feature size on our glass


https://doi.org/10.1021/acs.langmuir.1c02418
Langmuir 2021, 37, 14157−14166

photomask (5 $\mu$m) and (2) small variations in photoresist thickness across the sample due to the surface roughness of the Cu substrate. Polygons had a lower limit of 10 $\mu$m in lateral dimension because variations in photoresist thickness required a slight overexposure of the sample to ensure regions of thicker resist were completely exposed, and overexposure lead to corner rounding. Thus, only discs could be produced down to a 5 $\mu$m diameter with the current setup. Electron beam lithography could be used in future work to decrease the size of particles while maintaining the integrity of the desired particle shape. We foresee systematic variations in particle size from $<10^0$ to $\sim10^1$ $\mu$m could be used to help understand the self-alignment of nucleated single crystals at different stages of the CVD growth process of 2D materials on liquid catalysts.[57]

Notably, we could resolve diffusive behavior in particles as large as 50 $\mu$m in diameter (Figure 3e,f). The relative mean-squared displacement ($MSD_{Rel}$) as a function of lag time $\tau$ for a set of 50 $\mu$m discs was calculated using particle tracking algorithms[42] (Figure 3e) to extract the drift-corrected translational diffusivity $D_T = 0.024 \pm 0.012$ $\mu m^2/s$ using[43] $MSD_{Rel} = 8D_T\tau^{\alpha}$, where $\alpha = 0.98 \pm 0.19$. The reported errors are one standard deviation from the average of the $D_T$ and $\alpha$ values measured between lag times 10 s $\leq \tau \leq$ 20 s for the 14 independent $MSD_{Rel}$ curves obtained from the 14 pairs of particles tracked. At $\tau$ < 1 s the slope of the $MSD_{Rel}$ curve is ~0 because the motion of the particles cannot be resolved with the low numerical aperture objective used here (10×, NA = 0.30), but there are measurable displacements of the particles at $\tau$ > 10 s with this magnification. This is significant because the $D_T$ for our 50 $\mu$m diameter discs is of the same order of magnitude as the $D_T$ measured for silica spheres with a ~10× smaller diameter (4 $\mu$m) at an air−water interface.[58] This can be understood from the 2D dimensionality, where the mass of the graphene particles increases with the square of radius, while for spheroidal particles the mass increases with the cube of radius. Thus, the total mass of a 50 $\mu$m diameter graphene disc could fit in a 1.08 $\mu$m diameter graphene "sphere" (Supporting Information). Hence, monolayer 2D particles with diameters ≤10 $\mu$m, a convenient size for optical microscopy techniques, could be used to study thermally activated processes such as entropic ordering.[59] Figure 3f contains position vs time data for the six particles labeled in Figure 3e over a period of approximately 150 s. The displacements are Brownian in nature, with no evidence of directional motion or particle−particle interactions influencing particle trajectories.

**Analysis of Self-Assembled Structures.** The ability to make monodisperse samples enables application of conventional image analysis techniques that will help us understand how 2D particle size and shape influence the forces that drive interfacial self-assembly. We reiterate that the local assemblies of particles presented in this work most likely evolved from diffusion-limited aggregation, but the bulk area concentration could be manipulated via a Langmuir trough[45] in future work. IRM images of monolayer graphene discs with 10 $\mu$m diameter (Figure 4a) and 50 $\mu$m diameter (Figure 4c) were analyzed using the radial distribution function (RDF, $g(r/D_p)$, Figure 4b,d), where $r$ is the center-to-center separation between particles of diameter $D_p$, and the 2D fast Fourier transform (FFT, inset Figure 4b,d). The radial distribution function is a measure of the relative particle density of a system at a certain separation distance from a reference particle,[60] with a value of $g(r/D_p) > 1$ (<1) implying an excess (deficiency) of particles at a given separation distance, and the 2D FFT depicts the extent of order and orientational symmetry of a system by converting patterns within the image into the frequency domain.[60] Sharp, significant peaks were observed in the RDF for the 10 $\mu$m discs at dimensionless separation distances of ~1.2, ~2.3, and ~3.3 indicating that order extended to ~3 particle diameters from a reference particle (Figure 4b). Results from the 2D FFT image acquired from the assembly of 10 $\mu$m discs qualitatively agreed with the extent of order observed in the RDF, as there were ~3 hexagonal features present in the image (inset, Figure 4b); the hexagonal features imply hexagonal order within the assembly. In contrast, there was only one significant peak observed in the RDF for the 50 $\mu$m discs at a separation distance of ~1.2 (Figure 4d), and the 2D FFT image acquired for the 50 $\mu$m discs displayed minimal structural symmetry. The difference in structural order as a function of graphene disc size can be understood by the relative Brownian motion of particles of each size.

Small particles undergo increased Brownian motion relative to large particles (Figure 5), which allows small particles to explore more energy states in a system before becoming irreversibly attached to a neighboring particle via the van der Waals force. The ability to explore more energy states due to the increased Brownian motion gives smaller particles an entropic benefit to forming films with more ordered structures (i.e., "colloidal crystals"), whereas large particles may form more fractal-like structures due to lesser Brownian motion and stronger interparticle forces. We acknowledge the tendency of graphene particles to aggregate due to the lack of repulsive forces between particles currently prohibits the study of equilibrium structure formation for 2D particles with a particular size or shape. Future studies employing charged 2D particles such as $MoS_2$[25] or graphene oxide[61] could be used to understand the governing physics of nonaggregating, 2D particles and to understand if charged 2D particles form more ordered film structures than noncharged 2D particles. However, given that the functional properties of 2D particle films (i.e., conductivity, transparency, etc.) are intimately linked with film morphology,[62,63] our results in Figure 4 suggest that films with tailored structures and properties could be fabricated by simply varying the lateral size (or chemistry) of the particles used.

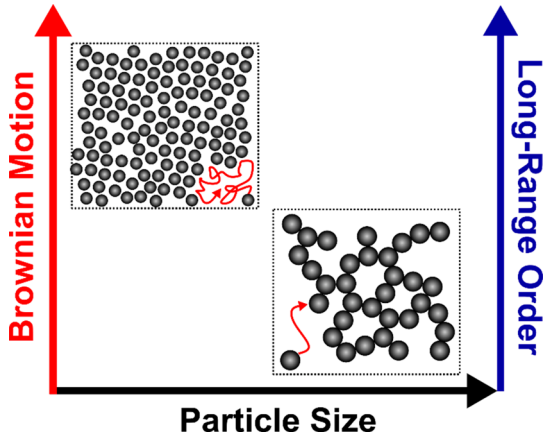


**Figure 5.** Schematic of the effect that particle size has on the Brownian motion and long-range structural order in systems of graphene discs.

In addition to Brownian motion yielding entropic benefits to the formation of films with greater structural order for 2D


https://doi.org/10.1021/acs.langmuir.1c02418
Langmuir 2021, 37, 14157−14166

particles with no distinct edges/corners (e.g., discs), further structural order can be achieved via directional shape entropy-driven forces for 2D particles with distinct edges (e.g., triangles, squares, etc.). IRM images of monolayer graphene triangles (25 $\mu$m), discs (50 $\mu$m), and squares (25 $\mu$m) at an air−water interface (Figure 6a−c) were analyzed using global

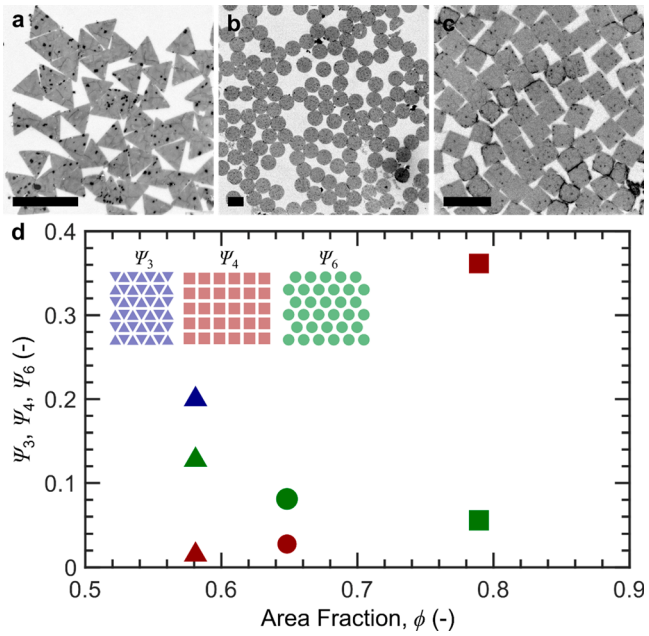


**Figure 6.** Analysis of self-assembled structures for different particle shapes. IRM image of (a) 25 $\mu$m triangle, (b) 50 $\mu$m discs, and (c) 25 $\mu$m squares at an air−water interface. Scale bars represent 50 $\mu$m. (d) Quantification of the 3-fold ($\Psi_3$, blue (triangles only)), 4-fold ($\Psi_4$, red), and 6-fold ($\Psi_6$, green) global bond order parameters as a function of the area fraction for each particle shape. Triangle, disc, and square markers correspond to the respective shape in (a−c). Inset image in (d) shows the maximum degree of order ($\Psi_n = 1$) for each global bond order parameter.

bond order parameters $\Psi_n$ ($n$ = 3, 4, 6, "Experimental" section) to determine the formation of ordered phases with $n$-fold angular order (Figure 6d).[13] A value of $\Psi_n = 1$ implies perfect $n$-atic order. At their respective area fraction $\phi$, triangles displayed triatic order ($\Psi_3 > \Psi_{4,6}$), discs displayed hexatic order ($\Psi_6 > \Psi_4$), and squares displayed quadratic order ($\Psi_4 > \Psi_6$). These results align with observations from simulations on hard 2D discs and polygons.[13,20] Given the magnitude of long-range, enthalpic interactions between 2D particles are $\leq 10^0$ $k_BT$,[25] and assuming our particles behave as hard 2D particles, the shape-induced order in these systems is likely of entropic origin.[20,59] Further evidence for shape entropy-induced[59] order can be seen when comparing $\Psi_6$ values for triangles and discs. The presence of distinct edges on triangular particles enables greater directional entropic forces, which manifests in greater order and a larger $\Psi_6$ for triangles than discs, even at lower triangle area fractions.[20] We note the size of the discs and triangles are different, and the reduced Brownian motion of 50 $\mu$m discs could also contribute to the lower $\Psi_6$ value. We also note that particles were not observed to rearrange after coming into close contact, which is in contrast to our previous work,[25] and can be explained by differences in particle lateral sizes (~1 $\mu$m[25] vs >10 $\mu$m diameter), their relative Brownian motion ("fast"[25] vs "slow"), and the shape of the particles (irregular[25] vs regular) used in the two works. Future work aimed at studying transient phenomena at specific area fractions using a Langmuir trough[45] will further illuminate the forces that drive the dynamics in these 2D colloidal systems and enable us to better understand how particle shape influences particle alignment (i.e., edge-to-edge vs corner-to-corner). Regardless, our results offer initial insight into the shape-regulated phase behavior of a truly 2D colloidal system, which has been previously limited to study by simulations and pseudo-2D experiments.

Finally, we acknowledge the slow dynamics of systems comprised of particles having lateral dimensions of 25 and 50 $\mu$m is a limitation in the current iteration of our model 2D colloidal system. Future work using particles with lateral dimensions $\leq$10 $\mu$m will enable the dynamical evolution of these systems to be studied at specific area fractions on more reasonable experimental time scales due to the greater Brownian motion of smaller particles.[25] However, current limitations in our photolithography-based fabrication technique prohibit the reliable fabrication of polygons with dimensions <10 $\mu$m, as noted in the discussion surrounding Figure 3, but could be remedied using higher resolution optical (e.g., direct-write) or electron beam lithography techniques.

## CONCLUSIONS

We have demonstrated a photolithography-based technique that enables fabrication of a system of one-atom-thick, 2D colloids: monolayer, size- and shape-controlled graphene particles at an air−water interface. Although not explicitly demonstrated here, these particles can be studied at liquid−liquid interfaces by simply adding a liquid upper phase.[25] A relation for the van der Waals force between two graphene discs interacting edge-to-edge was derived to explain the stability of the observed interfacial structures with evidence given by our ability to examine the same interfacial region before and after deposition from an air−water interface. A key aspect of our 2D colloids was the significant Brownian motion observed in particles with dimensions up to 50 $\mu$m. A lack of long-range forces coupled with extremely short-ranged van der Waals forces between particles enabled us to analyze our particles under the context of hard discs and polygons. Results suggest that particle shape influenced self-assembled structure via directional entropic forces.[59] Future efforts should focus on increasing shape fidelity through lithographic means such as optical direct-write photolithography or electron beam lithography to improve monodispersity in particle parameters. The significant advance of this work is the experimental realization of a truly 2D colloidal system;[7] a fluid−fluid interface acts as the 2D "fluid" dispersing our particles that have single-atom thickness, lateral dimensions large enough to be seen using optical microscopy yet still undergo significant Brownian diffusion, and physical parameters (e.g., size, shape, chemistry, and thickness) that can be easily manipulated. This work stands apart from previous experimental studies on pseudo-2D systems that relied on depletion to dampen $z$-direction translation of thin colloids[64] or ligand-functionalized nanoplatelets (lateral dimensions ~$10^0$ to $10^1$ nm, thicknesses ~$10^1$ nm) at fluid−fluid interfaces.[19] The tunability and functional properties of the new building blocks presented in this work provide a new means to experimentally study a plethora of fundamental physical processes and encourages future efforts aimed at rationally designing the assembly[34] of 2D particles for novel applications.[9]


https://doi.org/10.1021/acs.langmuir.1c02418
Langmuir 2021, 37, 14157−14166

## ■ ASSOCIATED CONTENT

### Supporting Information

The Supporting Information is available free of charge at https://pubs.acs.org/doi/10.1021/acs.langmuir.1c02418.

Use of methodology to fabricate monolayer $MoS_2$ particles, derivation of eq 2, Bond number analysis, comparison of the mass of a graphene disc to a graphene "sphere" (PDF)

## ■ AUTHOR INFORMATION


### Corresponding Author

**Joseph R. Samaniuk** − *Department of Chemical and Biological Engineering, Colorado School of Mines, Golden, Colorado 80401, United States;* orcid.org/0000-0002-6077-2999; Email: samaniuk@mines.edu

### Author

**David M. Goggin** − *Department of Chemical and Biological Engineering, Colorado School of Mines, Golden, Colorado 80401, United States;* orcid.org/0000-0001-6892-2034

Complete contact information is available at: https://pubs.acs.org/10.1021/acs.langmuir.1c02418



### Funding

NSF Faculty Early Career Development (CAREER) Program Award CBET-1944725.

### Notes

The authors declare no competing financial interest.


## ■ ACKNOWLEDGMENTS

D.M.G and J.R.S acknowledge the financial support of the NSF Faculty Early Career Development (CAREER) Program Award CBET-1944725.

## ■ REFERENCES


(1) Gasser, U.; Weeks, E. R.; Schofield, A.; Pusey, P. N.; Weitz, D. A. Real-Space Imaging of Nucleation and Growth in Colloidal Crystallization. *Science* **2001**, *292*, 258−262.

(2) Alsayed, A. M.; Islam, M. F.; Zhang, J.; Collings, P. J.; Yodh, A. G. Premelting at Defects Within Bulk Colloidal Crystals. *Science* **2005**, *309*, 1207−1210.

(3) Frenkel, D. Entropy-Driven Phase Transitions. *Phys. A* **1999**, *263*, 26−38.

(4) Zaccarelli, E. Colloidal Gels: Equilibrium and Non-Equilibrium Routes. *J. Phys.: Condens. Matter* **2007**, *19*, 50.

(5) Nguyen, V. D.; Faber, S.; Hu, Z.; Wegdam, G. H.; Schall, P. Controlling Colloidal Phase Transitions with Critical Casimir Forces. *Nat. Commun.* **2013**, *4*, 1584.

(6) Aarts, D.; Schmidt, M.; Lekkerkerker, H. N. W. Direct Visual Observation of Thermal Capillary Waves. *Science* **2004**, *304*, 847−850.

(7) Manoharan, V. N. Colloidal Matter: Packing, Geometry, and Entropy. *Science* **2015**, *349*, 1253751.

(8) Hwang, H.; Weitz, D. A.; Spaepen, F. Direct Observation of Crystallization and Melting with Colloids. *Proc. Natl. Acad. Sci. U. S. A.* **2019**, *116*, 1180−1184.

(9) Glotzer, S. C.; Solomon, M. J. Anisotropy of Building Blocks and Their Assembly into Complex Structures. *Nat. Mater.* **2007**, *6*, 557−562.

(10) van Anders, G.; Ahmed, N. K.; Smith, R.; Engel, M.; Glotzer, S. C. Entropically Patchy Particles: Engineering Valence through Shape Entropy. *ACS Nano* **2014**, *8*, 931−940.

(11) Sacanna, S.; Pine, D. J. Shape-Anisotropic Colloids: Building Blocks for Complex Assemblies. *Curr. Opin. Colloid Interface Sci.* **2011**, *16*, 96−105.

(12) Rossi, L.; Soni, V.; Ashton, D. J.; Pine, D. J.; Philipse, A. P.; Chaikin, P. M.; Dijkstra, M.; Sacanna, S.; Irvine, W. T. M. Shape-Sensitive Crystallization in Colloidal Superball Fluids. *Proc. Natl. Acad. Sci. U. S. A.* **2015**, *112*, 5286−5290.

(13) Avendaño, C.; Escobedo, F. A. Phase Behavior of Rounded Hard-Squares. *Soft Matter* **2012**, *8*, 4675−4681.

(14) Zhao, K.; Bruinsma, R.; Mason, T. G. Entropic Crystal−Crystal Transitions of Brownian Squares. *Proc. Natl. Acad. Sci. U. S. A.* **2011**, *108*, 2684−2687.

(15) Irvine, W. T. M.; Vitelli, V.; Chaikin, P. M. Pleats in Crystals on Curved Surfaces. *Nature* **2010**, *468*, 947−951.

(16) Wu, L.; Wang, X.; Wang, G.; Chen, G. In situ X-ray Scattering Observation of Two-Dimensional Interfacial Colloidal Crystallization. *Nat. Commun.* **2018**, *9*, 1335.

(17) Buhot, A.; Krauth, W. Phase Separation in Two-Dimensional Additive Mixtures. *Phys. Rev. E: Stat. Phys., Plasmas, Fluids, Relat. Interdiscip. Top.* **1999**, *59*, 2939−2941.

(18) Thapar, V.; Hanrath, T.; Escobedo, F. A. Entropic Self-Assembly of Freely Rotating Polyhedral Particles Confined to a Flat Interface. *Soft Matter* **2015**, *11*, 1481−1491.

(19) Ye, X.; Chen, J.; Engel, M.; Millan, J. A.; Li, W.; Qi, L.; Xing, G.; Collins, J. E.; Kagan, C. R.; Li, J.; Glotzer, S. C.; Murray, C. B. Competition of Shape and Interaction Patchiness for Self-Assembling Nanoplates. *Nat. Chem.* **2013**, *5*, 466−473.

(20) Anderson, J. A.; Antonaglia, J.; Millan, J. A.; Engel, M.; Glotzer, S. C. Shape and Symmetry Determine Two-Dimensional Melting Transitions of Hard Regular Polygons. *Phys. Rev. X* **2017**, *7*, 021001.

(21) Cote, L. J.; Kim, F.; Huang, J. X. Langmuir-Blodgett Assembly of Graphite Oxide Single Layers. *J. Am. Chem. Soc.* **2009**, *131*, 1043−1049.

(22) Biswas, S.; Drzal, L. T. A Novel Approach to Create a Highly Ordered Monolayer Film of Graphene Nanosheets at the Liquid-Liquid Interface. *Nano Lett.* **2009**, *9*, 167−172.

(23) Imperiali, L.; Liao, K. H.; Clasen, C.; Fransaer, J.; Macosko, C. W.; Vermant, J. Interfacial Rheology and Structure of Tiled Graphene Oxide Sheets. *Langmuir* **2012**, *28*, 7990−8000.

(24) Woltornist, S. J.; Oyer, A. J.; Carrillo, J. M. Y.; Dobrynin, A. V.; Adamson, D. H. Conductive Thin Films of Pristine Graphene by Solvent Interface Trapping. *ACS Nano* **2013**, *7*, 7062−7066.

(25) Goggin, D. M.; Zhang, H.; Miller, E. M.; Samaniuk, J. R. Interference Provides Clarity: Direct Observation of 2D Materials at Fluid−Fluid Interfaces. *ACS Nano* **2020**, *14*, 777−790.

(26) Silvera Batista, C. A.; Larson, R. G.; Kotov, N. A. Nonadditivity of Nanoparticle Interactions. *Science* **2015**, *350*, 1242477.

(27) Gardener, J. A.; Golovchenko, J. A. Ice-Assisted Electron Beam Lithography of Graphene. *Nanotechnology* **2012**, *23*, 185302.

(28) Li, W.; Moon, S.; Wojcik, M.; Xu, K. Direct Optical Visualization of Graphene and Its Nanoscale Defects on Transparent Substrates. *Nano Lett.* **2016**, *16*, 5027−5031.

(29) Israelachvili, J. N. *Intermolecular and Surface Forces*; Elsevier, 2011; pp 215−218.

(30) Kim, P. Y.; Gao, Y.; Chai, Y.; Ashby, P. D.; Ribbe, A. E.; Hoagland, D. A.; Russell, T. P. Assessing Pair Interaction Potentials of Nanoparticles on Liquid Interfaces. *ACS Nano* **2019**, *13*, 3075−3082.

(31) Lehle, H.; Oettel, M.; Dietrich, S. Effective Forces Between Colloids at Interfaces Induced by Capillary Wavelike Fluctuations. *Europhys. Lett.* **2006**, *75*, 174−180.

(32) Botto, L.; Lewandowski, E. P.; Cavallaro, M.; Stebe, K. J. Capillary Interactions Between Anisotropic Particles. *Soft Matter* **2012**, *8*, 9957−9971.

(33) Novoselov, K. S.; Mishchenko, A.; Carvalho, A.; Castro Neto, A. H. 2D Materials and Van der Waals Heterostructures. *Science* **2016**, *353*, aac9439.

(34) Millan, J. A.; Ortiz, D.; van Anders, G.; Glotzer, S. C. Self-Assembly of Archimedean Tilings with Enthalpically and Entropically Patchy Polygons. *ACS Nano* **2014**, *8*, 2918−2928.

(35) Bonaccorso, F.; Bartolotta, A.; Coleman, J. N.; Backes, C. 2D-Crystal-Based Functional Inks. *Adv. Mater.* **2016**, *28*, 6136−6166.
(36) Backes, C.; Higgins, T. M.; Kelly, A.; Boland, C.; Harvey, A.; Hanlon, D.; Coleman, J. N. Guidelines for Exfoliation, Characterization and Processing of Layered Materials Produced by Liquid Exfoliation. *Chem. Mater.* **2017**, *29*, 243−255.
(37) Li, Z.; Young, R. J.; Backes, C.; Zhao, W.; Zhang, X.; Zhukov, A.; Tillotson, E.; Conlan, A. P.; Ding, F.; Haigh, S. J.; Novoselov, K. S.; Coleman, J. N. Mechanisms of Liquid-Phase Exfoliation for the Production of Graphene. *ACS Nano* **2020**, *14*, 10976−10985.
(38) Nirmalraj, P. N.; Lutz, T.; Kumar, S.; Duesberg, G. S.; Boland, J. J. Nanoscale Mapping of Electrical Resistivity and Connectivity in Graphene Strips and Networks. *Nano Lett.* **2011**, *11*, 16−22.
(39) Lanza, M.; Smets, Q.; Huyghebaert, C.; Li, L.-J. Yield, Variability, Reliability, and Stability of Two-Dimensional Materials Based Solid-State Electronic Devices. *Nat. Commun.* **2020**, *11*, 5689.
(40) Uysal, A.; Zhou, H.; Feng, G.; Lee, S. S.; Li, S.; Cummings, P. T.; Fulvio, P. F.; Dai, S.; McDonough, J. K.; Gogotsi, Y.; Fenter, P. Interfacial Ionic 'Liquids': Connecting Static and Dynamic Structures. *J. Phys.: Condens. Matter* **2015**, *27*, 032101.
(41) Zhou, H.; Uysal, A.; Anjos, D. M.; Cai, Y.; Overbury, S. H.; Neurock, M.; McDonough, J. K.; Gogotsi, Y.; Fenter, P. Understanding Defect-Stabilized Noncovalent Functionalization of Graphene. *Adv. Mater. Interfaces* **2015**, *2*, 1500277.
(42) Crocker, J. C.; Grier, D. G. Methods of Digital Video Microscopy for Colloidal Studies. *J. Colloid Interface Sci.* **1996**, *179*, 298−310.
(43) Samaniuk, J. R.; Vermant, J. Micro and Macrorheology at Fluid-Fluid Interfaces. *Soft Matter* **2014**, *10*, 7023−7033.
(44) Eckmann, A.; Felten, A.; Mishchenko, A.; Britnell, L.; Krupke, R.; Novoselov, K. S.; Casiraghi, C. Probing the Nature of Defects in Graphene by Raman Spectroscopy. *Nano Lett.* **2012**, *12*, 3925−3930.
(45) Kale, S. K.; Cope, A. J.; Goggin, D. M.; Samaniuk, J. R. A Miniaturized Radial Langmuir Trough for Simultaneous Dilatational Deformation and Interfacial Microscopy. *J. Colloid Interface Sci.* **2021**, *582* (Pt. B), 1085−1098.
(46) Goggin, D. M.; Bei, R.; Anderson, R.; Gomez-Gualdron, D. A.; Samaniuk, J. R. Stacking of Monolayer Graphene Particles at a Water-Vapor Interface. *J. Phys. Chem. C* **2021**, *125*, 7880−7888.
(47) Chiou, Y.-C.; Olukan, T. A.; Almahri, M. A.; Apostoleris, H.; Chiu, C. H.; Lai, C.-Y.; Lu, J.-Y.; Santos, S.; Almansouri, I.; Chiesa, M. Direct Measurement of the Magnitude of the Van der Waals Interaction of Single and Multilayer Graphene. *Langmuir* **2018**, *34*, 12335−12343.
(48) Lee, J.; Nakouzi, E.; Xiao, D.; Wu, Z.; Song, M.; Ophus, C.; Chun, J.; Li, D. Interplay between Short- and Long-Ranged Forces Leading to the Formation of Ag Nanoparticle Superlattice. *Small* **2019**, *15*, 1901966.
(49) Bian, X.; Kim, C.; Karniadakis, G. E. 111 Years of Brownian Motion. *Soft Matter* **2016**, *12*, 6331−6346.
(50) Liu, I. B.; Sharifi-Mood, N.; Stebe, K. J. Capillary Assembly of Colloids: Interactions on Planar and Curved Interfaces. *Annu. Rev. Condens. Matter Phys.* **2018**, *9*, 283−305.
(51) Stamou, D.; Duschl, C.; Johannsmann, D. Long-Range Attraction Between Colloidal Spheres at the Air-Water Interface: The Consequence of an Irregular Meniscus. *Phys. Rev. E: Stat. Phys., Plasmas, Fluids, Relat. Interdiscip. Top.* **2000**, *62*, 5263−5272.
(52) Goggin, D. M.; Samaniuk, J. R. Dynamics of Pristine Graphite and Graphene at an Air-Water Interface. *AIChE J.* **2018**, *64*, 3177−3187.
(53) Zheng, Q. B.; Ip, W. H.; Lin, X. Y.; Yousefi, N.; Yeung, K. K.; Li, Z. G.; Kim, J. K. Transparent Conductive Films Consisting of Ultra Large Graphene Sheets Produced by Langmuir-Blodgett Assembly. *ACS Nano* **2011**, *5*, 6039−6051.
(54) Wojcik, M.; Li, Y. Q.; Li, W.; Xu, K. Spatially Resolved In Situ Reaction Dynamics of Graphene via Optical Microscopy. *J. Am. Chem. Soc.* **2017**, *139*, 5836−5841.
(55) Wang, Y. F.; Wang, Y.; Breed, D. R.; Manoharan, V. N.; Feng, L.; Hollingsworth, A. D.; Weck, M.; Pine, D. J. Colloids with Valence and Specific Directional Bonding. *Nature* **2012**, *491*, 51−U61.
(56) Bradley, L. C.; Chen, W. H.; Stebe, K. J.; Lee, D. Janus and Patchy Colloids at Fluid Interfaces. *Curr. Opin. Colloid Interface Sci.* **2017**, *30*, 25−33.
(57) Geng, D. C.; Yu, G. Liquid Catalysts: An Innovative Solution to 2D Materials in CVD Processes. *Mater. Horiz.* **2018**, *5*, 1021−1034.
(58) Boniello, G.; Blanc, C.; Fedorenko, D.; Medfai, M.; Ben Mbarek, N.; In, M.; Gross, M.; Stocco, A.; Nobili, M. Brownian Diffusion of a Partially Wetted Colloid. *Nat. Mater.* **2015**, *14*, 908.
(59) van Anders, G.; Klotsa, D.; Ahmed, N. K.; Engel, M.; Glotzer, S. C. Understanding Shape Entropy Through Local Dense Packing. *Proc. Natl. Acad. Sci. U. S. A.* **2014**, *111*, E4812−E4821.
(60) Mac Fhionnlaoich, N.; Qi, R.; Guldin, S. Application of the Spatial Distribution Function to Colloidal Ordering. *Langmuir* **2019**, *35*, 16605−16611.
(61) Silverberg, G. J.; Pearce, P.; Vecitis, C. D. Controlling Self-Assembly of Reduced Graphene Oxide at the Air-Water Interface: Quantitative Evidence for Long-Range Attractive and Many-Body Interactions. *ACS Appl. Mater. Interfaces* **2015**, *7*, 3807−3815.
(62) Fahimi, A.; Jurewicz, I.; Smith, R. J.; Sharrock, C. S.; Bradley, D. A.; Henley, S. J.; Coleman, J. N.; Dalton, A. B. Density Controlled Conductivity of Pristine Graphene Films. *Carbon* **2013**, *64*, 435−443.
(63) Kim, H.; Mattevi, C.; Kim, H. J.; Mittal, A.; Mkhoyan, K. A.; Riman, R. E.; Chhowalla, M. Optoelectronic Properties of Graphene Thin Films Deposited by a Langmuir-Blodgett Assembly. *Nanoscale* **2013**, *5*, 12365−12374.
(64) Wang, P. Y.; Mason, T. G. A Brownian Quasi-Crystal of Pre-Assembled Colloidal Penrose Tiles. *Nature* **2018**, *561*, 94.


https://doi.org/10.1021/acs.langmuir.1c02418
*Langmuir* 2021, 37, 14157−14166